Characterization of High-performance Exfoliated Natural Rubber/Organoclay Nanocomposites

Peiyao Li,[1,2] Li Wang,[1] Guojun Song,[1,2] Lanlan Yin,[3] Feng Qi,[1] Liangdong Sun[1]

[1]*Institute of Polymer Materials, Qingdao University, Qingdao 266071, China*
[2]*College of Materials Science and Engineering, Beijing University of Chemical Technology, Beijing 100029, China*
[3]*Haidu College of Qingdao Agricultural University, Laiyang 265200, China*

Received 26 November 2007; accepted 30 March 2008
DOI 10.1002/app.28480
Published online 6 June 2008 in Wiley InterScience (www.interscience.wiley.com).

ABSTRACT: The exfoliated natural rubber (NR)/organoclay nanocomposites were successfully prepared with an optimal organoclay by direction blending. The optimal-type organoclay was chosen by characterization of XRD and the mechanical properties characterization of the NR/organoclay composites from three kinds of organoclay. The observation of transmission electron microscopy (TEM) revealed well-ordered exfoliated single layers of organoclay. The results of mechanical properties measurement showed that the tensile strength, tensile modulus, and tear strength were improved remarkably with small amounts of organoclay, whose contents were below 5.0 phr. For example, incorporating with 3.0 phr organoclay, the tensile strength and tear strength of nanocomposite were 24.7 MPa and 34.7 kN/m, respectively, which increased ~ 89.5% and 61.6%. Furthermore, the results of coreinforcement system with high performance indicated a promising application of the organoclay and nanocomposites. The values of the weight-swelling ratio of nanocomposites decreased much, which meant the oil resistance of nanocomposites enhanced. The TGA results indicated that the thermal stability of nanocomposites was improved. The reduction of oxygen permeability implied the gas-barrier properties of the nanocomposites improved. Furthermore, the mechanism of barrier of clay layers was discussed. © 2008 Wiley Periodicals, Inc. J Appl Polym Sci 109: 3831–3838, 2008

Key words: natural rubber; organoclay; nanocomposite; mechanical properties; gas permeability

INTRODUCTION

Polymer/layered silicate nanocomposites were defined as materials in which the particle size of the dispersed phase was nanometer sized at least in one dimension.[1] This nanocomposite exhibited outstanding properties of modulus, strength and barrier, improvement of solvent and heat resistance, and decrease of flammability.[2–5] The clay for nanocomposites usually needed to be organically modified, which aimed to improve the compatibility of polymer and organoclay layers, and which would enlarge the space of the layers to be more accessible to the intercalation of polymer chains. Since the first nanocomposite was prepared and characterized,[6] it provided a new technological and economic route for the production with high performance only incorporating a small percentage of organoclay, and it led to a new era of nanocomposites. From then onward, the works about organoclay, as a reinforcer, were already introduced in various polymer materials, such as for the plastics, polyamide,[7,8] polypropylene,[9,10] polystyrene,[11] polycarbonate,[12] and poly(ethylene terephthalate)[13]; and the rubbers, NBR,[14] CR,[15] HNBR,[16] SBR,[17] silicone elastomer,[18] and BR.[19] The previous studies showed that the organoclay had been proven to be a very effective reinforcement in both thermoplastic and thermoset polymer materials.

Natural rubber (NR) was a conventional rubber with wide use in many applications such as inner tube, tubing, and balloon. Recently, the studies of NR/clay nanocomposites were mostly by latex with sodium montmorillonite clay slurry[5,20,21] or incorporating large amounts of organoclay above 10 phr[4,22]; which would greatly increase the cost of the manufacturing products. This study focused on investigating the NR/organoclay nanocomposites incorporating with small amounts of organoclay below 5.0 phr. It was expected to exploit novel nanocomposites with high performance. In the beginning, several types of organoclay were filled into NR to find out the optimal organoclay by mechanical properties measurements. X-ray diffraction (XRD) experiments were done to determine the interlayer space of three kinds of organoclay and the optimal organoclay in the NR matrix. The morphologies of the optimal organoclay dispersed in NR matrix were characterized by transmission electron microscopy (TEM). The stress–strain behavior, tensile strength, and tear strength of NR/organoclay nanocomposites were

Correspondence to: P. Li (polymerlpy@hotmail.com).

tested and discussed. The effect of organoclay on thermal stability of nanocomposite was characterized by TGA. Solvent penetrability and oxygen permeability measurement were used to investigate the solvent resistance and gas-barrier property of nanocomposite, respectively. Summarizing the experiments results, we expected to discuss the mechanism of barrier effect of clay layers.

EXPERIMENTAL

Materials

The used NR was the Thailand Standard ribbed smoke sheet No. 3 (RSS3) grade NR. The organoclay named Nos. I, II, and III was prepared as mentioned in the following page, which were produced in Institute of Polymer Materials of Qingdao University, China. Carbon black, calcium carbonate, talcum powder, and porcelain clay were conventional commercial products. The vulcanization curatives: stearic acid (S_A), zinc oxide (ZnO), sulfur (S), and 2-mercaptobenzothiazole (M) were also commercial products. The used recipe was as follows (in parts), rubber: 100 g; organoclay: various; ZnO: 5.0 g; S_A: 1.0 g; M: 1.8 g; and S: 1.5 g.

Preparation of Organophilic Montmorillonite (OMMT)

The raw clay obtained from the bentonite mine was wetted with water and then purified by sedimentation, washing, and drying. The fined clay (50 g) was dispersed into 1000 mL of distilled water at 68°C under vigorous stirring. A mixture of 35 g dodecyl amine (or 50 g hexadecyl amine or 95 g didodecyl methyl amine), 10 mL 98% concentrated sulfuric acid was prepared at 65°C and then added into the montmorillonite dispersion. The reaction was maintained for 2 h (or 4 or 7 h). The sediment was collected by filtration and washed with water and then dried in vacuum; after ground and sieved; the organophilic clay was designated as Organoclay I or II or III.

Preparation of composites

The mixing process took place on a two-roll miller incorporating with organoclay or other fillers and the other ingredients with a nip clearance of 0.8 mm and friction ratio 1.3 (22/17 rpm). Mixing was performed at room temperature for 5–10 min. The specimens of ~ 2-mm thickness were vulcanized in a hot press at 145°C and 20 MPa pressure for 30 min. The vulcanized sheets were laid aside at room temperature for 24 h, and then they were used to measure the performances.

Measurement

According to standard ISO37-1994 and ISO34-1:1994, respectively, vulcanized composites sheets were cut into standard samples. On dumbbell-shaped and crescent-shaped specimens, the tensile properties and tear strength were determined by using an electronic Universal Testing Machine (D and G Company, China) at a crosshead speed of 500 mm/min. All measurements were made with 10 samples, and the values were averaged; the reported results were at room temperature tests.

XRD experiments were performed for the pristine clay and the organoclay using a D/max-RB diffractometer (Rigaku, Japan), which has an X-ray generator of 12 kW, a graphite monochromator, Cu Kα radiation (wavelength, $\lambda = 0.154$ nm) and operating at 40 kV, 100 mA. The samples were scanned at a scanning speed of 5°/min under the diffraction angle 2θ of 1°–30°.

Sample was thin sectioned with an ultramicrotome. Sections were collected on a copper grid and examined with a TEM (JEM-1200EX), which produced from Japanese JEOL Company running at an accelerating voltage of 80 kV.

An Akron type abrasion tester(Tianfa Company, China) was used to evaluate the abrasion properties of the composites according to Chinese National Standard GB/T 1689-1998. The weight loss of the specimen wheel was obtained after a rolling distance of 1610 m, and the abrasion volume (mL/1.61 km) was calculated by dividing the weight loss by the density of the composite specimen.

A PE7 dynamic mechanical thermal analyzer (PE Company, America) was used to evaluate the dynamic elastic modulus (E') and loss tangent (tan δ) of the nanocomposites. The PE7 experimental setup was based on a single tensile mode. The frequency was 1 Hz with 3°C/min scanning rate, and the strain was 0.5%. A temperature range from −100 to 50°C was used to obtain the glass transition temperature.

According to the International Standard ISO 2556-2001, the permeation experiment of oxygen was carried out with gas permeability measuring apparatus (YANACO Company, Japan). The specimens of nanocomposite, containing 3.0 phr organoclay, had a diameter of 8 cm and thickness of about 1 mm. The rate of transmission of oxygen was obtained by gas chromatography, and the oxygen permeability was calculated from it.

The samples of $20 \times 10 \times 2$ mm^3 were used to determine the swelling behavior of vulcanized rubber according to ISO 1817-198. The initial weight of the samples was taken, and then they were put into toluene. The samples were periodically removed from the test bottles, the adhering solvent was

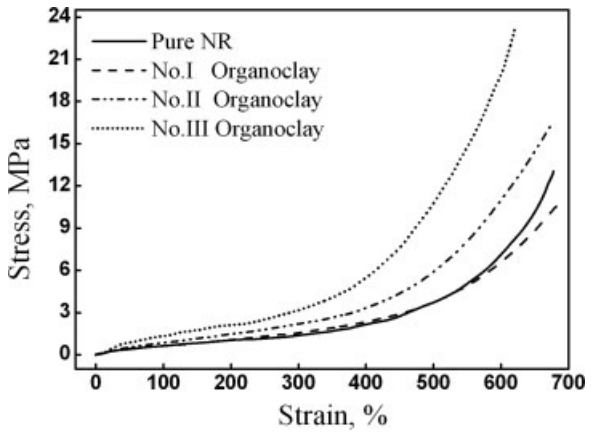

Figure 1 Stress–strain curves of pure NR and composites with 3.0 phr organoclay I, II, and III.

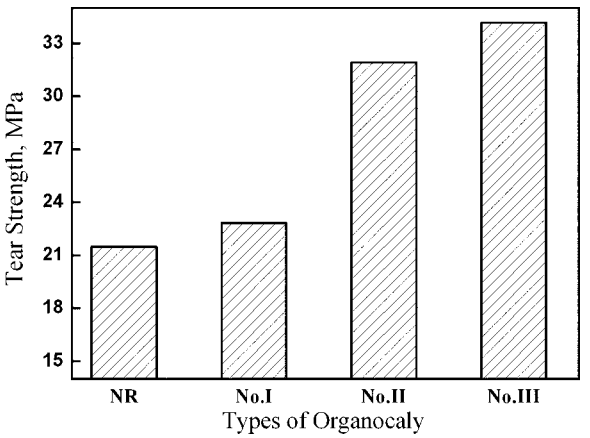

Figure 2 Tear strength of pure NR and composites with 3.0 phr organoclay I, II, and III.

cleaned from the surface, and the samples were weighed immediately and then placed into the toluene again. The weight-swelling ratio, Q_t, was also determined from the weight of the sample in the unswollen and swollen states. The equation as the following:

$$Q_t = \frac{\Delta M}{M_0} = \frac{M_t - M_0}{M_0} \times 100$$

where Q_t is the weight-swelling ratio, M_t the weight of the sample in the swollen states, and M_0 the initial weight of the samples.

Thermogravimetric analyses (TGA) were performed on a TGA/STDA851^e instrument, which produced from Mettler-Toledo Company with platinum pan using $\sim$ 7 mg of material as probe. The samples were heated at 10°C/min rate under nitrogen atmosphere under a flow rate of 50 mL/min.

RESULTS AND DISCUSSION

The selection of the optimal organoclay

The stress–strain curves of crosslinked pure NR and composites samples with 3.0 phr three types organoclay were shown in Figure 1. It clearly showed that the tensile modulus of the composites with organoclay II and III were higher than that of pure NR and No. I composite. During the elongation closing the broken areas, the two curves had the characteristic of dramatic increase in tensile modulus, and the tensile strength was higher than that of the others. The composites containing organoclay(III) had the highest tensile strength. The effects of organoclay types on the tear strength of the crosslinked NR/organoclay composites were illustrated in Figure 2. The column graphs showed that there was slight increase of the tear strength of the composites with organoclay(I) and that of the composites with organoclay II or III was higher than pure NR; moreover, the composites with organoclay(III) also had the highest tear strength than others. Thus, it was noted that the organoclay(III) had the best reinforcement effect on NR, and then the optimal organoclay to study NR/organoclay nanocomposites was the organoclay(III).

Characterization of organoclay

The organoclay was prepared as described earlier. As a result, the surface of the organoclay had organic characteristics. The hydrophobic organic modifier could facilitate the intercalation of a hydrophobic polymer into clay by reducing the surface energy.

The XRD patterns of pristine clay and organoclay I, II, and III were shown in Figure 3. The interlayer distance was determined from the diffraction peak position in the XRD, using the Bragg's equation. The basal distance of pristine clay and the interlayer distances of organoclay I, II, and III were 1.56, 1.80, 2.08, and 3.39 nm, respectively. It was clear that the

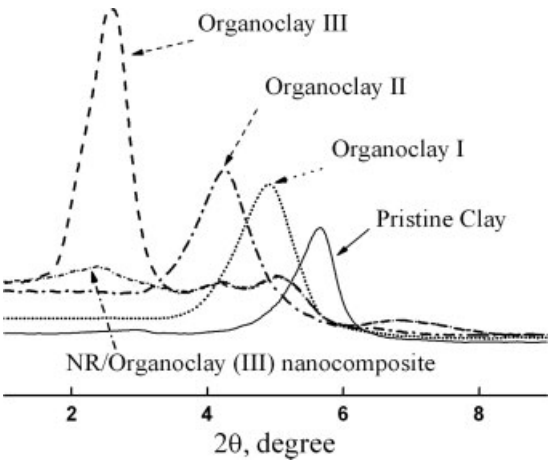

Figure 3 X-ray diffraction patterns of pristine clay, organoclay I, II, III, and NR/organoclay(III) nanocomposite.

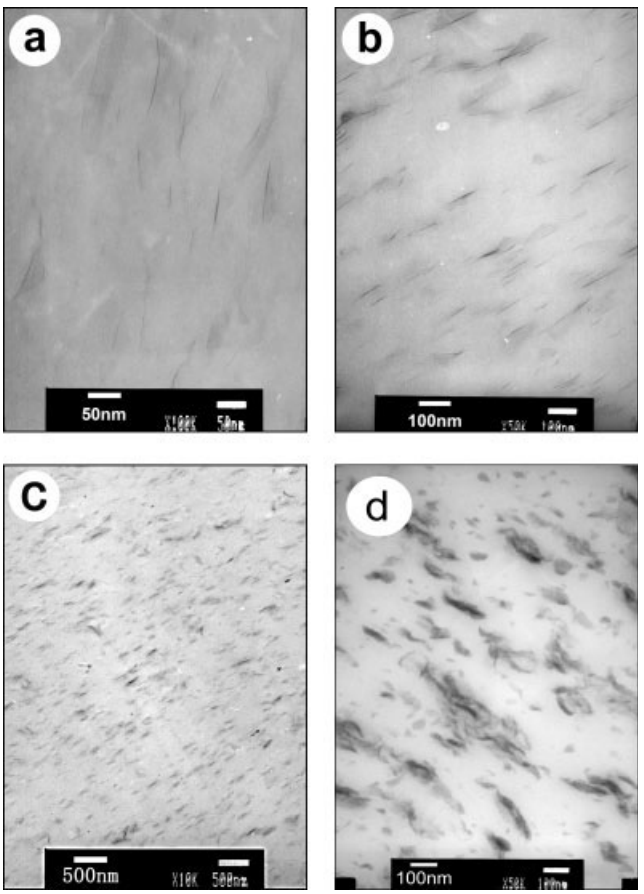

Figure 4 TEM images for NR/organoclay(III) nanocomposite (3.0 phr): (a) 100 K magnification. TEM images for NR/Organoclay(III) nanocomposite (3.0 phr); (b) 50 K magnification. TEM images for NR/organoclay(III) nanocomposite (3.0 phr); (c) 25 K magnification. TEM images for NR/organoclay(III) nanocomposite (5.0 phr); (d) 50 K magnification.

intercalation of organic modifier enlarges the distance of the clay layers that suggests the successful preparation of organoclay, and it showed that the organoclay III had the best intercalation of modifier. The great enlargement of layers' space of organoclay III would give more chances for the intercalation of macromolecular chains. In addition, the XRD patterns of NR/organoclay(III) nanocomposites were measured in Figure 3. It showed there was no the characterized peak of organoclay(III) in the nanocomposites, which meant the organoclay(III) had exfoliated in the nanocomposites. Furthermore the morphology of organoclay(III) in the nanocomposites would be observed in the following TEM section.

TEM micrographs of NR/organoclay(III) nanocomposites

Observation of TEM was used to reveal the morphology of the organoclay in the composites to distinguish the type of the composites. TEM images

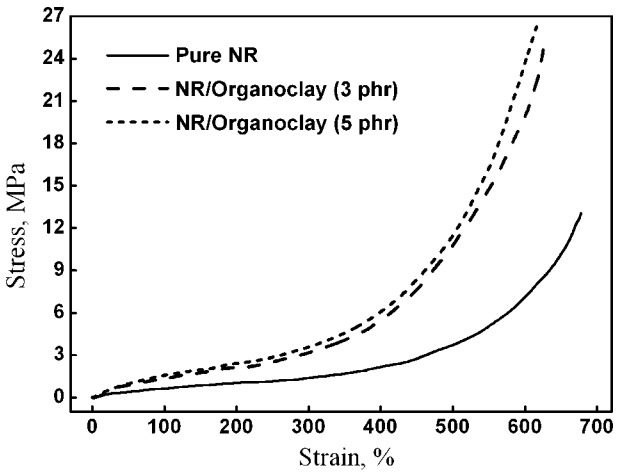

Figure 5 The stress–strain behavior of NR/organoclay(III) nanocomposites with various organoclay contents.

had been screened at high and low magnification to observe the dispersion of organoclay in the NR matrix; they were presented in Figure 4; and Figure 4(a)–(c) contains 3.0 phr organoclay(III). In the images, the light-color place was NR matrix, and the dark lines were the single-clay layers. The submicroscopic structure in detail of nanocomposites was presented in Figure 4(a,b) at 50 and 100-nm scale bar, respectively. Figure 4(a,b) clearly shows the exfoliated single-clay layers. Furthermore, the interface of the organoclay layers and the matrix was indistinct that indicated the good compatibility of organoclay layers and the matrix. Figure 4(c) with 500-nm scale bar showed the dispersion of organoclay in the matrix at low magnification, which could be taken the comprehensive observation in a large scope. From the observations of the above three TEM photos, only the exfoliated single layers could be seen; there were no multilayer bundles or aggregates. That meant that the uniformly exfoliated NR/organoclay

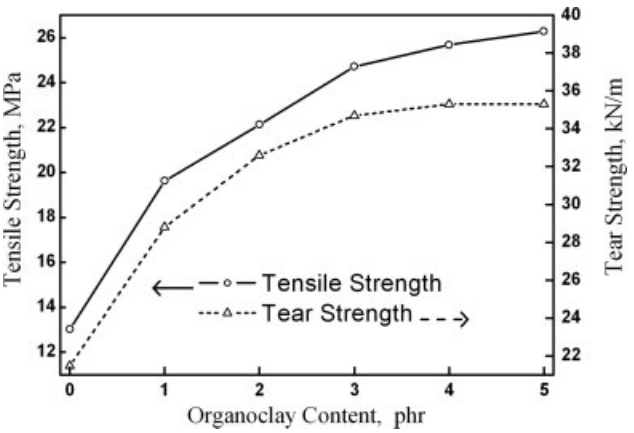

Figure 6 Curves of tensile strength and tear strength versus organoclay content (phr) of NR/organoclay(III) nanocomposites.

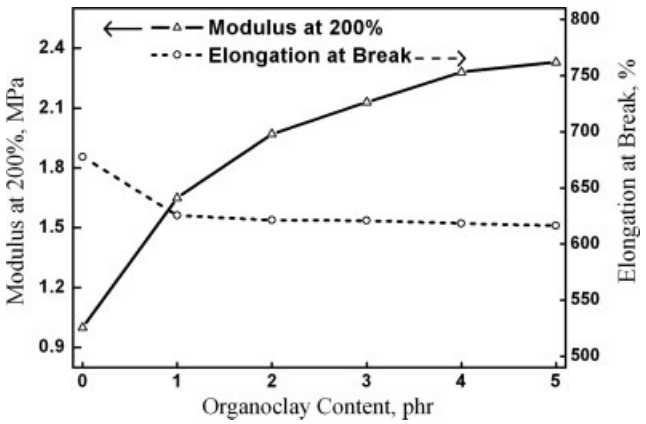

Figure 7 Curves of modulus at 200% and elongation at break versus organoclay content (phr) of NR/organoclay(III) nanocomposites.

nanocomposites were prepared. But in Figure 4(d) with 5.0 phr organoclay, it showed the organoclay aggregated, so in the following pages, the effect of the multilayers would be discussed.

Mechanical properties of NR/organoclay(III) nanocomposites

Figure 5 represented the stress–strain curves of pure NR and NR/organoclay(III) nanocomposites on various organoclay(III) contents. The curve of pure NR demonstrated a typical stress induced crystallization behavior; it showed that the modulus of rubber was low and slowly increased with the increase of strain in the lower strain region; and then the stress would sharply increase within a small strain range due to the development of tensile crystallization. The nanocomposites with 3.0 and 5.0 phr organoclay(III) had slight difference of tensile behavior. As shown in Figure 5, the modulus and tensile strength of nanocomposites were higher than those of pure NR, and the stress transition caused by tensile crystallization clearly weakened; it showed that the stress was smoothly increasing; it was possibly caused by the nanometer effect of nanodispersed organoclay layers, which increased the force between the layers and the NR macromolecular chain, and then reduced the occurrences of tensile crystallization.[20]

Figure 6 shows the increase in trend of tensile strength and tear strength of nanocomposites with various organoclay contents. It showed that the tensile strength and tear strength all remarkably improved, that is, the strengths increased to 24.7 MPa and 34.7 kN/m with 3.0 phr organoclay contents, respectively. They enhanced as much as 89.5% and 61.6% relative to that of pure NR, respectively. The improvement of the strengths indicated the super reinforcement of organoclay. Above the 3.0 phr contents, the slowdown of the improvement rate of the two strength was due to the poor dispersion of organoclay, for example, as Figure 4(d) shown with 5.0 phr organoclay(III), the partial multilayered organoclay would enhance the strength little.

Figure 7 represented the modulus at 200% and the elongation at break of nanocomposites with various organoclay contents. As shown in Figure 5, Figure 7 shows the modulus at 200% gradually improved with the increase in the addition of organoclay. It was believed that the improvement of modulus was caused by the interaction of organoclay layers and the NR macromolecular chains. The results of elongation at break showed that it decreased slightly relative to the pure NR. It was possibly caused by the reduction of tensile crystallization.

The so-called coreinforcement system contained small amounts organoclay(III) and a lot of conventional fillers in the rubber matrix. The mechanical properties of the coreinforcement were reported in Table I. The properties were given in terms of the modulus at different strains (100 and 300%), the tensile strength and elongation at break, tear strength, and abrasion resistance. It showed that the composites only with 3.0 phr organoclay(III) had the better properties than the composites completely filled with conventional fillers at the same fillers contents. For the necessary addition of conventional fillers, the enhancement of coreinforcement composites indicated a promising application of NR/organoclay nanocomposites.

TABLE I
Mechanical Properties of Coreinforcement Composites

	CB (50 phr)	OC/CB (3 + 47 phr)	CC (50 phr)	OC/CC (3 + 47 phr)	TP (50 phr)	OC/TP (3 + 47 phr)	PC (50 phr)	OC/PC (3 + 47 phr)
Modulus at 100% (MPa)	2.0	2.6	1.1	1.4	1.3	1.9	1.3	2.0
Modulus at 300% (MPa)	8.0	13.0	2.4	4.3	2.1	4.2	2.0	3.0
Tensile strength (MPa)	15.8	22.3	15.2	22.1	16.8	20.8	15.1	19.4
Elongation at break (%)	427.3	436.6	645.9	605.9	723.4	576.1	654.5	633.5
Tear strength (MPa)	24.9	46.7	23.7	28.9	24.0	29.8	22.4	26.1
Wear volume	437	361	3311	2340	3424	1720	3874	2074

OC, organoclay(III); CB, carbon black; TP, talcum powder; CC, calcium carbonate; PC, porcelain clay.

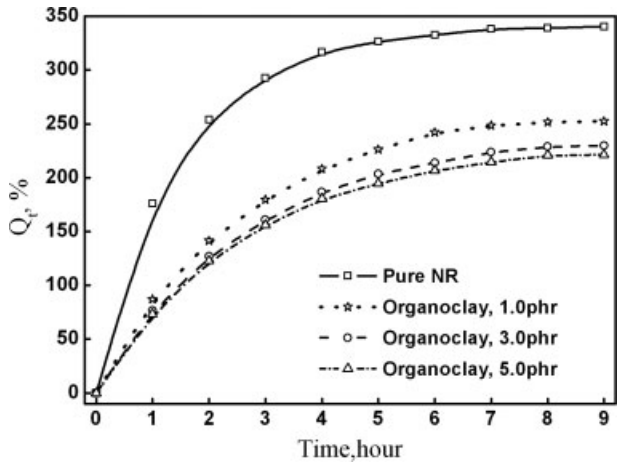

Figure 8 Swelling behavior of NR/organoclay(III) nanocomposites in toluene at 20°C.

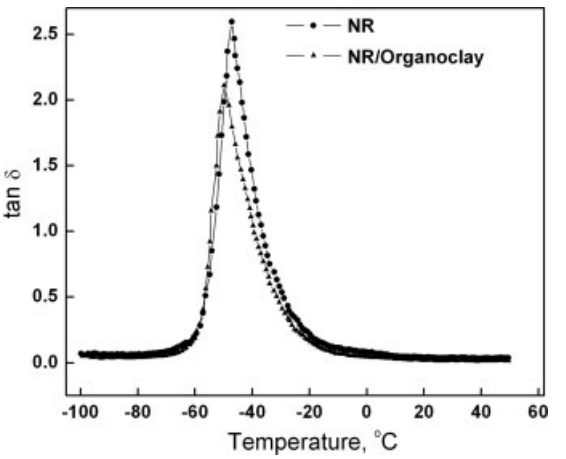

Figure 10 The relation of the loss tangent of pure NR and NR/organoclay(III) nanocomposite versus the temperature.

Swelling behavior of NR/organoclay(III) nanocomposites

The sorption curves of nanocomposites filled with 1.0, 3.0, and 5.0 phr organoclay(III) versus time obtained by plotting Q_t (the weight-swelling ratio) in toluene at room temperature were shown in Figure 8. It showed that the solvent absorption decreased with the contents of clay increasing. The rate of solvent absorption was due to the presence of the nanodispersed impermeable clay layers, which decreased the rate of transportation by lengthening the average diffusion path length in NR matrix.

Dynamic properties of NR/organoclay(III) nanocomposites

The samples of pure NR and NR/organoclay(III) nanocomposite containing 3.0 phr organoclay(III) were tested by dynamic mechanical thermal analysis (Figs. 9 and 10). As presented in Figure 9, below the glass transition temperature (T_g), there was slight increase for the storage modulus of NR/organoclay nanocomposite compared to pure NR. Above the T_g, the nanocomposite showed the similar modulus values compared to pure rubber. The temperature corresponding to tan δ_{max} could be thought of as the glass transition temperature (T_g) of NR material, which was about -50°C. Based on Figure 10, it could be seen that there was a small decrease in the tan δ_{max} of nanocomposite compared to pure rubber.

Thermal stability of NR/organoclay(III) nanocomposites

Figure 11 showed the TGA curves for pure NR and NR/organoclay(III) nanocomposite with 3.0 and 5.0 phr organoclay(III) contents. The inserted figure in Figure 11 was the curves of differential calculus of TGA curves, which was used to find out the temper-

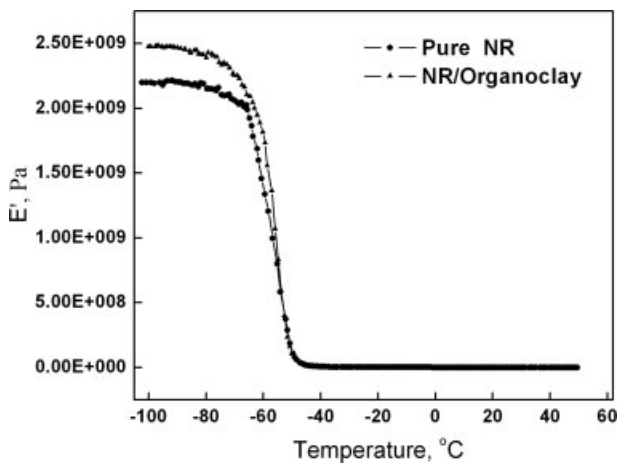

Figure 9 The relation of the storage modulus of pure NR and NR/organoclay(III) nanocomposite versus the temperature.

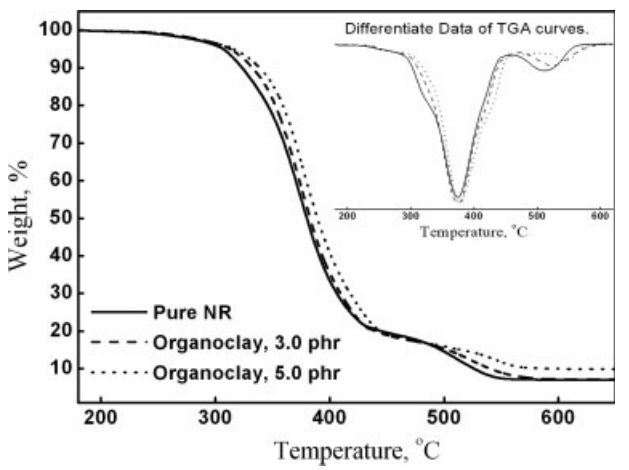

Figure 11 TGA curves of Pure NR, NR/organoclay(III) nanocomposites with 3.0 and 5.0 phr organoclay.

TABLE II
Temperatures of Weight Loss of Pure NR and Nanocomposites

	$T_{i-5\ wt\%}$ (°C)	$T_{i-10\ wt\%}$ (°C)	$T_{max\ 1}$ (°C)	$T_{max\ 2}$ (°C)
Pure NR	306.4	323.7	373.8	510.3
NR/organoclay(III) (3.0 phr)	313.1	332.8	374.4	523.0
NR/organoclay(III) (5.0 phr)	316.1	339.1	377.6	544.6

ature of maximum deposition rate ($T_{max.1}$ and $T_{max.2}$). The initial thermal stability (T_i) was characterized by the temperatures at 5 and 10 wt % weight loss ($T_{i-5\ wt\%}$ and $T_{i-10\ wt\%}$), which were tabulated in Table II. It could be seen that the T_i of nanocomposites increased remarkably relative to the pure NR. This meant that the initial thermal stability of nanocomposites had improved. The values of T_{max} showed in Table II were higher than those of pure NR. The results of deposition temperature measurement indicated that the heat resistance of nanocomposite was improved.

Gas barrier of NR/organoclay(III) nanocomposites

Reducing gas-permeation rates were an important research area of polymer materials. Based on the results shown in Table III, it showed that the nanocomposite containing 3.0 phr organoclay(III) had a clear decrease of oxygen permeability; the value of permeability reduced as much as 49.4% compared to the pure NR. The results meant that the gas-barrier properties of nanocomposites improved much.

Mechanism of the barrier effect of organoclay layers in nanocomposites

Figure 12 was cut from Figure 4 TEM photos; it was used to describe the barrier mechanism of clay layers. It was supposed that the molecules wanted to enter or pass through the material from I to II or III. As shown in the figure, the moving path would be longer than the simulative path; which was much longer than the vertical distance between the two points. That meant that the practical movement distance was prolonged, which would reduce the quantity of the passed molecules. So, the nanodispersed layers formed the ''barrier'' to improve the barrier properties of the material. The existence of nanodispersed clay layers improved the barrier properties was called ''multi-path effect'' or ''nano-wall effect.''[3]

TABLE III
The Results of the Oxygen Permeability of Pure NR and NR/Organoclay(III) Nanocomposite Containing 3.0 phr Organoclay

Samples	Pure NR	NR/organoclay(III) nanocomposite
Oxygen Permeability ($cm^3\ m^{-2}$ 24 h Pa)	2.39×10^{-2}	1.21×10^{-2}

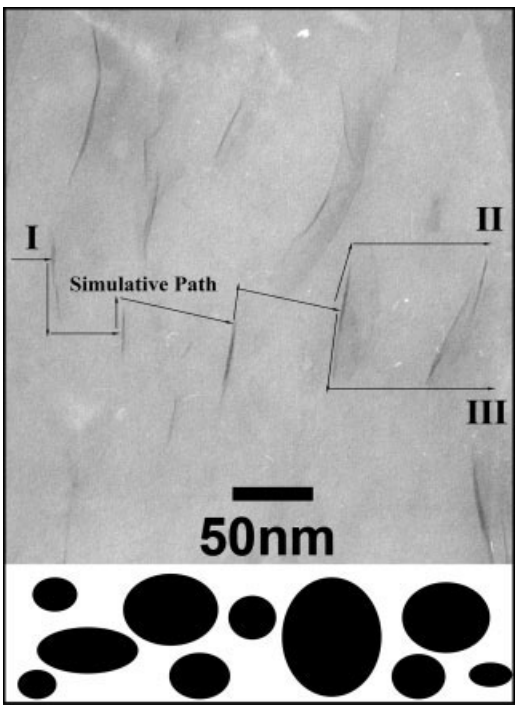

Figure 12 The schematic figures of barrier mechanism of clay layers.

CONCLUSIONS

This work devoted to investigating the NR/organoclay nanocomposites by direction blending. The following conclusions could be drawn:

- The space of layers of the optimal organoclay was greatly increased by organic modification.
- It was confirmed that the exfoliated NR/organoclay nanocomposite was successfully prepared with the uniform dispersion of organoclay single layers by XRD and TEM observations.
- The mechanical properties testing results showed that the tensile strength and tear strength of nanocomposite were 24.7 MPa and 34.7 kN/m, respectively, which increased $\sim$ 89.5% and 61.6%. It revealed the wonderful reinforcement effect of organoclay.
- The swelling-behavior testing and the TGA showed the oil resistance, and the thermal stability of nanocomposites was greatly improved.
- The discussed mechanism of barrier effect could be used to explain the improvement of the barrier properties of the nanocomposites.

The authors thank the experts in TEM observation laboratory for helping in preparing and testing the samples for this study. The authors thank the reviewer for critical comments to improve the quality of this work.

References

1. Karger K. J.; Zhang Z. In Mechanical Properties of Polymers Based on Nanostructure and Morphology; Calleja, J.F.B., Michler, G.H., Eds. New York: Marcel Dekker, in press.
2. Chang, J.-H.; An, Y. U.; Kim, S. J.; Im, S. Polymer 2003, 44, 5655.
3. Usuki, A.; Hasegawa, N.; Kadoura, H.; Okamoto, T. Nano Letters 2001, 1, 271.
4. Wu, Y.-P.; Wang, Y.-Q.; Zhang, H.-F.; Wang, Y.-Z.; Yu, D.-S.; Zhang, L.-Q.; Yang, J. Compos Sci Technol 2005, 65, 1195.
5. Varghese, S.; Karger-Kocsis, J. Polymer 2003, 44, 4921.
6. Okada, A.; Kawasumi, M.; Kurauchi, T. Polym Prepr 1987, 28, 447.
7. Liu, L.; Qi, Z.; Zhu, X. J Appl Polym Sci 1999, 71, 1133.
8. Shelley, J. S.; Mather, P. T.; DeVries, K. L. Polymer 2001, 42, 5849.
9. Sun, T.; Garces, J. M. Adv Mater 2002, 14, 128.
10. Gianelli, W.; Ferrara, G.; Camino, G. Polymer 2005, 46, 7037.
11. Serge, B.; Jeffrey, W. G.; Charles, A. W. Polym Degrad Stab 2004, 84, 483.
12. Stretz, H. A.; Koo, J. H.; Dimas, V. M.; Zhang, Y. Polym Prepr 2001, 42, 50.
13. Ou, C. F.; Ho, M. T.; Lin, J. R. J Polym Res 2003, 10, 127.
14. Hwang, W. G.; Wei, K. H.; Wu, C. M. J Polym 2004, 45, 5729.
15. Sridhar, V.; Tripathy, D. K. J Appl Polym Sci 2006, 101, 3630.
16. Gatos, K. G.; Sawanis, N. S.; Apostolov, A. A. Macromol Mater Eng 2004, 289, 1079.
17. Zhang, Z. J.; Zhang, L. N.; Li, Y.; Xu, H. D. Polymer 2005, 46, 129.
18. LeBaron, P. C.; Pinnavaia, T. J. Chem Mater 2001, 13, 3760.
19. Wang, S. H.; Zhang, Y.; Ren, W. T.; Zhang, Y. X.; Lin, H. F. Polym Test 2005, 24, 766.
20. Wang, Y. Q.; Zhang, H. F.; Wu, Y. P.; Yang, J.; Zhang, L. Q. Eur Polym J 2005, 41, 2776.
21. Stephen, R.; Varghese, S.; Joseph, K.; Oommen, Z.; Thomas, S. J Membr Sci 2006, 282, 162.
22. Arroyo, M.; Lopez-Manchado, M. A.; Herrero, B. Polymer 2003, 44, 2447.